Pergamon

Acta Astronautica Vol. 44, No. 5, pp. 227–241, 1999

Printed in Great Britain
0094-5765/99 $ - see front matter

PII: S0094-5765(99)00021-1

CHARACTERIZATION OF THE OPTIMAL MASS PROBLEM FOR AEROBRAKING TETHERS

J.M. LONGUSKI†, S.G. TRAGESSER
School of Aeronautics and Astronautics, Purdue University, West Lafayette, IN, 47907-1282, USA

and

J. PUIG-SUARI
Department of Mechanical and Aerospace Engineering, Arizona State University, Tempe, AZ, 85287-6101, USA

(Received 27 August 1996)

Abstract—In the aerobraking tether concept, a probe, connected to an orbiter by a long, thin tether, passes through the atmosphere of a target planet to provide a desired velocity change, while keeping the orbiter above the sensible atmosphere. In earlier work, simple analytic models have been developed which accurately describe the characteristics of the mass-optimal tether. In this paper these models are generalized so that design of the spacecraft and the aerobraking maneuver can be completely characterized by four independent parameters. By comparing the tether mass (e.g. for aerocapture) with the propellant mass required to capture the orbiter, we show that aerobraking tethers have a clear advantage for a wide range of maneuvers. © 1999 Elsevier Science Ltd. All rights reserved

1. INTRODUCTION

As an alternative to chemical propulsion, the aerobraking tether is proposed as a means to decelerate a spacecraft at atmosphere-bearing planets. The spacecraft is comprised of a probe (or lander) and an orbiter connected by a long, thin tether. During the maneuver, the probe flies through the atmosphere to provide the necessary braking, while the tether allows the orbiter to remain at a certain altitude, or clearance, above the probe to eliminate aerodynamic effects (Fig. 1).

The first mention of the concept of an aerobraking tether in the literature appears to be by Carroll [1], although the idea was being discussed at the Jet Propulsion Laboratory at least as early as 1984 by Sirlin *et al.* [2]. Another early reference to the aerobraking tether concept is made by Purvis and Penzo [3].

There are many important papers which deal with the general problem of a tether in an atmosphere. Here we refer to Lorenzini *et al.* [4], Bergamaschi and Bonon [5], Keshmiri and Misra [6], Gullahorn [7], Krischke *et al.* [8], Pasca and Lorenzini [9], Bae *et al.* [10] and Warnock and Cochran [11]. (For a more general treatment of tethers in space see the handbook by Penzo and Ammann [12] and the first book on space tether systems by Beletsky and Levin [13].)

†Corresponding author. Tel.: +1-765-494-5139; fax: +1-765-494-0307; e-mail: longuski@ecn.purdue.edu.

The first demonstration of the physical feasibility of using aerobraking tethers is presented by Puig-Suari and Longuski [14,15]. They model the tether as a rigid rod subject to distributed aerodynamic and gravitational forces and show that the orbiter altitude can be maintained above the sensible atmosphere during the aerobraking maneuver.

There are several papers which address the design of aerobraking tethers and the aerobraking maneuver. The *vertical dumb-bell maneuver* is considered in [16] in which the tether flys through the atmosphere in, roughly, the local vertical orientation. Several design criteria are applied to minimize normal forces on the tether (in order to minimize bending when the tether model includes flexibility effects [17,18]). For example, the area of the probe is chosen so the ballistic coefficient of the tether and probe are equal (i.e. *aeromatched*) [16]. The design rules are applied to the major atmosphere-bearing bodies in the solar system (Venus, Earth, Mars, Jupiter, Saturn, Titan, Uranus and Neptune). In every case, the resulting mass of the tether is significantly lower than the propellant required to achieve aerocapture. The efficacy of these design rules in minimizing bending is demonstrated in [17,19].

Numerical, quasi-gradient optimization techniques are employed in [20] to determine if the vertical dumb-bell design yields the optimum tether mass. It was discovered that the vertical dumb-bell maneuver is optimal in some cases, but often the minimum mass tether is achieved with a maneuver

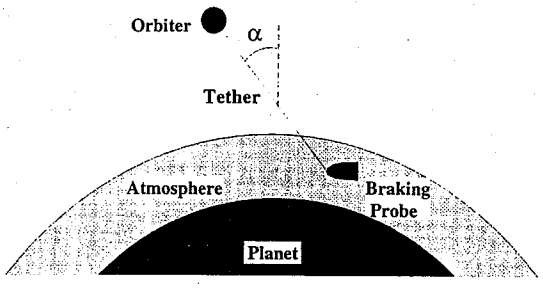

Fig. 1. Aerobraking tether.

in which the tether is tilted away from the local vertical. This *inclined maneuver* requires a longer tether to obtain clearance, but the forces can be dramatically reduced, resulting in a net reduction in tether mass. The parameter optimization is improved upon in [21,22] by mapping the cost function (tether mass) for varying initial conditions.

Two analytical models are developed in [16,20] to characterise the two optimal maneuvers that emerged from numerical investigation. The *vertical impact model* (VI) gives an approximation of the tether mass for the vertical dumb-bell maneuver, based on an impulsive drag force. The *sliding pendulum model* (SP) is used to approximate the inclined maneuver (by analogy) with the equations of motion of a rigid pendulum with a sliding attachment point. In [22], these models are used to show that the optimal mass problem is a function of three parameters: the mass ratio of the probe to the orbiter, $m_r = m_p/m_o$, the required altitude clearance, $\bar{h}_c = h_c/H$ (in scale heights, H), and a nondimensional speed variable:

$$u \equiv (\Delta V/V_{lc})\sqrt{2\pi r_{\text{per}}/(He)}$$

where ΔV is the required change in velocity for aerobraking, V_{lc} is the local circular velocity, r_{per} is the radius of periapsis and e is the approach eccentricity. Figure 2 illustrates the results when one of these parameters, the speed variable u, is varied. The circles in the figure represent the mass optimal solution from a precise numerical optimization using the equations of motion from [14,15]. The nondimensional mass, $\tilde{m}_t$, is defined by

$$\tilde{m}_t = m_t \Big/ \left(\frac{m_o V_{lc}^2 eH\rho}{2\pi r_{\text{per}}\sigma}\right)$$

where m_t is the tether mass, m_o is the orbiter mass, ρ is the density per unit volume of the tether and σ is the ultimate strength per unit area. In the figure we see remarkable agreement between the theoretical predictions and the numerical results. The letters J, N, S, U, V, E, T and M stand for aerobraking at Jupiter, Neptune, Saturn, Uranus, Venus, Earth, Titan and Mars, respectively. We notice the numerical solutions for J, N, S and U lie on the dashed curve corresponding to the vertical impact model, while V, E, T and M follow the sliding pendulum model very closely. When we consider large variations of each of the three parameters u, $\bar{h}_c$, m_r (while the other two are constrained to finite, nonzero quantities), we can summarize the results of [22] by the following observations:

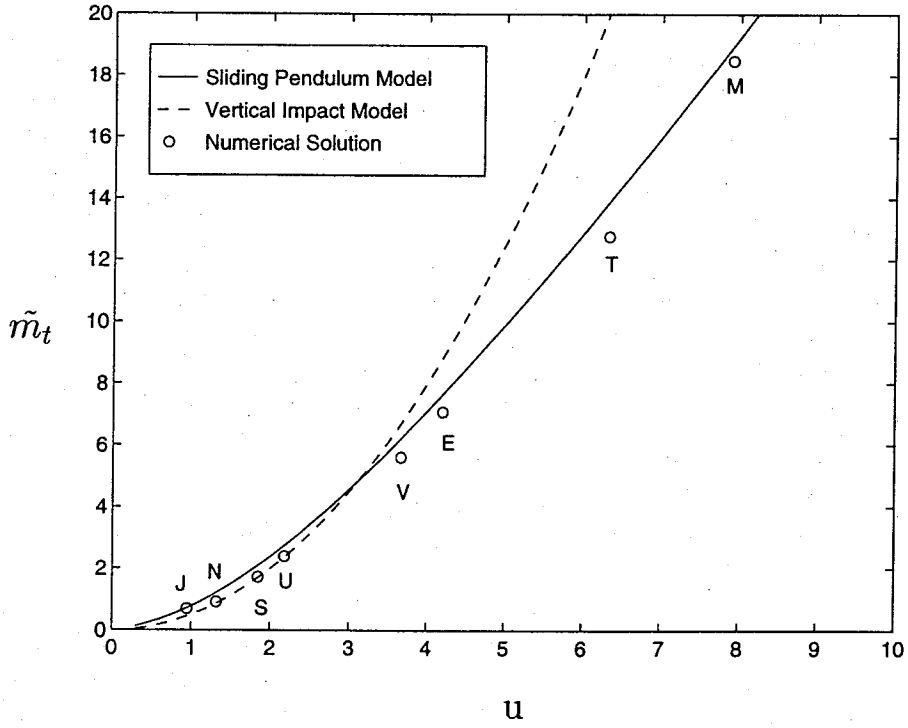

Fig. 2. Theoretical and numerical tether mass ($m_r = 1$, $\bar{h}_c = 1.8$).

1. The optimal mass maneuver approaches a vertical dumb-bell maneuver when u decreases, $\bar{h}_c$ increases or m_r increases.
2. The optimal mass maneuver approaches an inclined maneuver when u increases, $\bar{h}_c$ decreases or m_r decreases.

These analytic models were developed for the cases where the tether mass was much smaller than the total system mass [22]. Unfortunately, this assumption limits the scope of investigation since the tether mass can become quite large (e.g. when the ΔV is large). In this paper we extend the theory to cover *massive tethers*. In conjunction with earlier work [14–22], this provides a general approach to designing the tether system and the aerobraking maneuver through the introduction of a fourth nondimensional scaling parameter [23].

2. VERTICAL DUMB-BELL AND INCLINED MANEUVERS

The aerobraking maneuver is illustrated in Fig. 3. The tethered system arrives at the target planet spinning clockwise (opposite to the orbital motion). As the probe enters the atmosphere, aerodynamic torque decreases the spin rate of the system until the tether reaches its minimum orientation angle, $\alpha_{\min}$. At this point, drag on the probe begins to spin the tether in the opposite direction. To minimize the forces on the tether, the magnitude of the spin rate leaving the atmosphere should be roughly equal to the spin rate entering the atmosphere (a design concept referred to as *spin matching* [16]).

The time histories of the orientation angle, α, and the forces exerted on the probe end of the tether for typical examples of the vertical dumb-bell and inclined maneuvers (Jupiter and Mars, respectively) are shown in Figs 4 and 5. In each of these cases, the tether is launched from Earth to the target planet via a Hohmann transfer. The simulations shown in Figs 4 and 5 start from a point outside the atmosphere, reach periapsis at about 250 s and terminate when the system is completely out of the sensible atmosphere at 500 s. The final orbit, after aerobraking, has an eccentricity of 0.9999. The *clearance requirement* is that the minimum altitude of the orbiter be at least 1.8 H (scale heights) above the minimum altitude of the probe. The solutions shown provide the minimum tether mass, which in each case is significantly less than the propellant mass required to capture the orbiter.

The optimal tether mass solution for Jupiter is the vertical dumb-bell maneuver shown in Fig. 4. This maneuver is characterized by the vertical orientation of the tether at closest approach; consequently, drag at periapsis acts in a direction normal to the tether and the tension is zero at this point (when $t = 240$ s). Thus the maximum tension is due to the spinning of the tether outside of the atmosphere. Note that the normal forces are nearly zero due to careful consideration of the system design parameters [16].

The inclined maneuver, which is optimal at Mars, never reaches a vertical orientation during closest approach, so $\alpha_{\min} > 0$. For the case at Mars, we find from Fig. 5 that $\alpha_{\min} = 40°$. This inclined orientation at periapsis, where aerodynamic forces are very large, results in an axial component of drag along the tether. As a result, the tension history reaches its maximum value during the atmospheric fly through (when t ranges between 150 and 350 s).

In the next sections, models are developed to provide insight into the dynamics of the aerobraking tether and to give a rough approximation for the minimum tether mass. The characteristics of the two maneuver types just described are very different, warranting two different models, namely the *vertical impact model* (for vertical dumb-bell maneuvers) and the *sliding pendulum model* (for inclined maneuvers).

3. VERTICAL IMPACT MODEL FOR MASSIVE TETHERS

Since the maximum tension of the vertical dumb-bell maneuver occurs outside the atmosphere (due to spin rate), the tether mass can be estimated by modeling the atmospheric fly-through as an impact problem, as discussed in [16]. In this previous investigation, the tether was designed for small ΔVs, so the tether mass was assumed to be much less than the system mass. The resulting approximation for

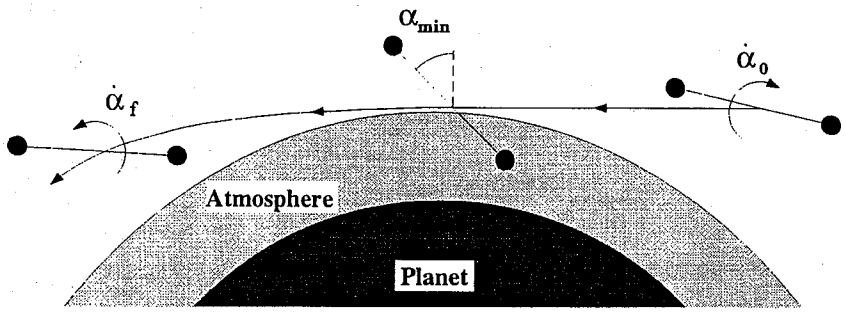

Fig. 3. Aerobraking maneuver.

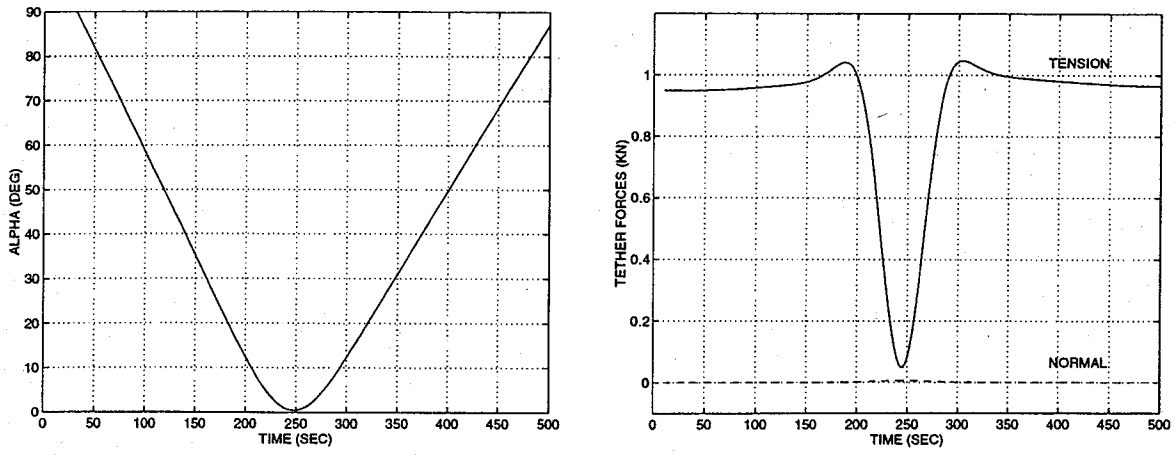

Fig. 4. Orientation angle and forces of vertical dumb-bell maneuver (Jupiter).

the tether mass is not accurate for the range of maneuvers we are now considering.

By allowing for massive tethers in the vertical impact model (VI), we encounter two major differences. First of all, the tension is now dependent on the tether mass (which is dependent on the tension) so the equation for the mass is transcendental. Second, the tension due to spin rate varies along the length of the tether since the tether must now support its own weight in addition to the end masses. Consequently, a tapered tether yields the lowest tether mass. Since a simple expression for tether mass is desired, we avoid this complication and restrict our discussion to tensions at the endbodies (probe and orbiter) of a uniform tether. (For a detailed discussion of the tapered tether problem, see [24].)

To determine the expression for the tether mass, we assume all the aerodynamic drag acts impulsively on the probe, as shown in Fig. 6. The impulse, P, is found from the principle of linear impulse and linear momentum:

$$P = (m_t + m_o + m_p)\Delta V \tag{1}$$

where m_t, m_o and m_p are the masses of the tether, orbiter and probe, respectively, and ΔV is the change in velocity of the system center of mass. The linear impulse, P, causes an angular impulse that is equal to the change in angular momentum so we have

$$Pl_p = (m_t + m_o + m_p)\Delta V l_p = I\Delta\Omega \tag{2}$$

where $\Delta\Omega$ is the change in the angular velocity and I is the system inertia about the center of mass, given by [16]:

$$I = m_o l_o^2 + m_p l_p^2 + m_t(l_o^3 + l_p^3)/(3l) \tag{3}$$

where l_o and l_p are the distances from the orbiter and probe, respectively, to the center of mass and are given by:

$$l_o = l(m_p + m_t)/m$$
$$l_p = l(m_o + m_t)/m \tag{4}$$

where l is the total tether length and m is the total system mass.

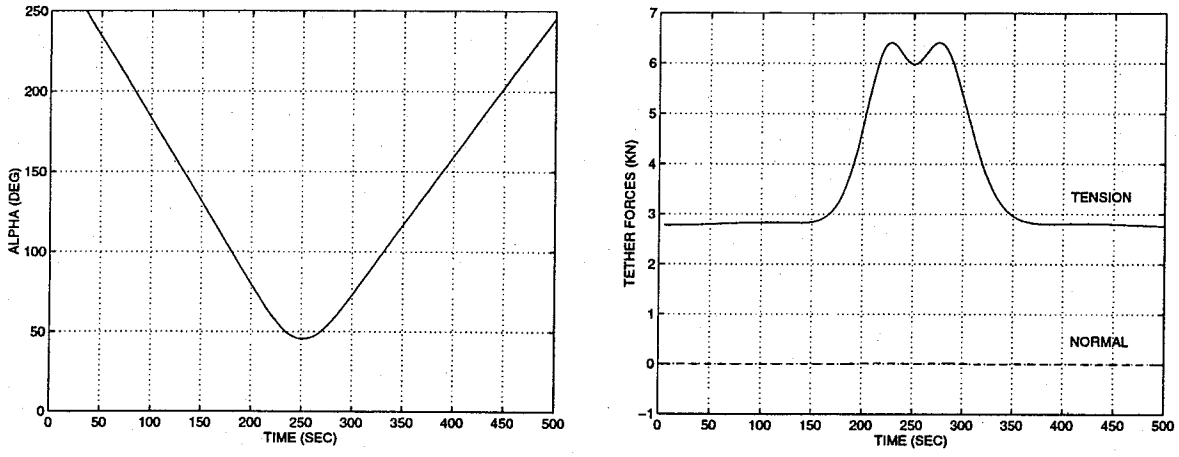

Fig. 5. Orientation angle and forces of inclined maneuver (Mars).

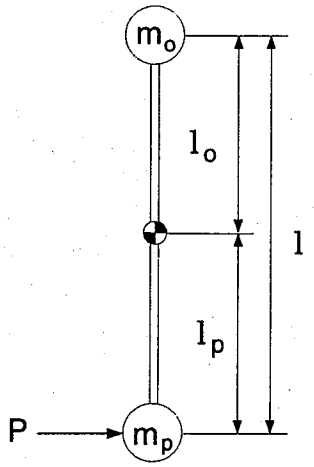

Fig. 6. Vertical impact model.

In order to minimize the tension on the tether we design the aerobraking maneuver so the angular velocity before impact and the angular velocity after impact are equal. Thus, the maximum spin rate is

$$\Omega_{\max} = \Delta\Omega/2 = m\Delta V l_p/(2I). \tag{5}$$

The maximum tensions on the probe and orbiter, $(T_p)_{\max}$ and $(T_o)_{\max}$, respectively, due to the spin rate are

$$(T_p)_{\max} = m_p l_p \Omega_{\max}^2 = \frac{m_p m^2 l_p^3}{4I^2}\Delta V^2$$

$$(T_o)_{\max} = m_o l_o \Omega_{\max}^2 = \frac{m_o l_o m^2 l_p^2}{4I^2}\Delta V^2. \tag{6}$$

The calculation of the tether mass is obtained by making the tether just strong enough to withstand the spin tension. We then have a tether mass approximation, m_{tp}, based on the tension at the probe, and another, m_{to}, based on the tension at the orbiter:

$$m_{tp} = (T_p)_{\max} l\rho/\sigma = \frac{m_p m^2 l_p^3 l\rho}{4I^2\sigma}\Delta V^2$$

$$m_{to} = (T_o)_{\max} l\rho/\sigma = \frac{m_o m^2 l_o l_p^2 l\rho}{4I^2\sigma}\Delta V^2 \tag{7}$$

where ρ is the density per unit volume of the tether and σ is the ultimate strength per unit area. If Eqs. (3) and (4) are substituted into eqn (7), the tether length, l, cancels out; that is, the tether mass for the vertical dumb-bell maneuver is independent of tether length. (The reason for this cancellation is discussed in [16].) To show this independence explicitly, we define the following mass ratios

$$\bar{m}_t \equiv m_t/m_o, \quad m_r \equiv m_p/m_o \tag{8}$$

and a set of nondimensional parameters that are functions of these two ratios only:

$$\bar{m} \equiv m/m_o = 1 + m_r + \bar{m}_t$$
$$\bar{l}_o \equiv l_o/l = (m_r + \bar{m}_t)/(1 + m_r + \bar{m}_t)$$
$$\bar{l}_p \equiv l_p/l = (1 + \bar{m}_t)/(1 + m_r + \bar{m}_t)$$
$$\bar{I} \equiv I/(m_o l^2) = \left[\frac{(m_r + \bar{m}_t)}{(1 + m_r + \bar{m}_t)}\right]^2 + m_r\left[\frac{(1 + \bar{m}_t)}{(1 + m_r + \bar{m}_t)}\right]^2 + \bar{m}_t/12. \tag{9}$$

Thus, the ratio of the tether mass to orbiter mass, $\bar{m}_t$, can be written as a function of the two mass ratios and ΔV only (assuming fixed tether characteristics, ρ and σ):

$$\bar{m}_{tp} = m_{tp}/m_o = \frac{m_r \bar{m}^2 \bar{l}_p^3 \rho}{4\bar{I}^2\sigma}\Delta V^2 = f_p(\bar{m}_{tp}, m_r, \Delta V)$$

$$\bar{m}_{to} = m_{to}/m_o = \frac{\bar{m}^2 \bar{l}_o \bar{l}_p^2 \rho}{4\bar{I}^2\sigma}\Delta V^2 = f_o(\bar{m}_{to}, m_r, \Delta V) \tag{10}$$

where $\bar{m}_{tp}$ and $\bar{m}_{to}$ are the tether mass ratios determined from the probe and orbiter tensions, respectively. Note that Eqs. (10) are transcendental because $\bar{l}_o$, $\bar{l}_p$ and $\bar{I}$ are all functions of $\bar{m}_t$. They can be solved numerically using a root finder to obtain $\bar{m}_{tp}$ and $\bar{m}_{to}$ for given m_r and ΔV.

Taking the ratio of Eqs. (10) yields

$$\frac{\bar{m}_{tp}}{\bar{m}_{to}} = m_r \frac{l_p}{l_o} = m_r \frac{(1 + \bar{m}_t)}{(m_r + \bar{m}_t)}. \tag{11}$$

Defining

$$m_r \equiv 1 + \epsilon \tag{12}$$

the ratio in eqn (11) can be written as

$$\frac{\bar{m}_{tp}}{\bar{m}_{to}} = 1 + \frac{\epsilon \bar{m}_t}{1 + \epsilon + \bar{m}_t}. \tag{13}$$

This ratio is unity only in the special case that the probe and orbiter have equal masses (i.e. $\epsilon = 0$) or the unrealistic case of $\bar{m}_t = 0$. Otherwise, the larger of the two mass predictions is chosen since the tether must be made to withstand the maximum tension. If the probe mass is larger than the orbiter mass ($m_r > 1$), then $\epsilon > 0$ and the ratio in eqn (13) is greater than one. Consequently, the prediction based on the probe tension, $\bar{m}_{tp}$, has a larger value. On the other hand, for $m_r < 1$ (but greater than or equal to zero by a physical argument) we have $-1 \leqslant \epsilon < 0$ and the tether mass ratio in eqn (13) is less than one, indicating that $\bar{m}_{to}$ is larger than $\bar{m}_{tp}$. The resulting tether mass prediction for the vertical impact theory can be summarized as

$$\bar{m}_t = \begin{cases} \bar{m}_{tp} & \text{if } m_r > 1 \\ \bar{m}_{tp} = \bar{m}_{to} & \text{if } m_r = 1 \\ \bar{m}_{to} & \text{if } m_r < 1 \end{cases} \tag{14}$$

where $\bar{m}_{tp}$ and $\bar{m}_{to}$ are calculated using Eqs. (10).

Note that if we neglect the tether mass in the expressions for l_o, l_p and I, then Eqs. (7) simplify im-

mediately to the result given in [16]:

$$m_t = \frac{m_o(m_o + m_p)\rho}{4m_p\sigma}\Delta V^2. \tag{15}$$

For cases where the optimal aerobraking maneuver is a vertical dumb-bell, eqn (14) yields fairly accurate results (typically within about 10% of the numerically optimized solution).

4. SLIDING PENDULUM MODEL FOR MASSIVE TETHERS

Since the maximum tension of the inclined maneuver occurs *during* the atmospheric fly-through, the impact model does not provide a suitable approximation for the tether mass. A more realistic representation of the drag force is required. Longuski *et al.* [20] and Tragesser *et al.* [22] provide surprisingly accurate estimates of the optimal tether mass with a sliding pendulum model (SP). In the model, a rigid pendulum with a sliding attachment point (see Fig. 7) is subjected to a forcing function that exponentially decreases with increasing altitude. The sliding pendulum model accurately represents behavior previously observed in simulation of optimal maneuvers; namely, the orbiter remains at a constant altitude during the atmospheric fly-through while the probe "swings down" to achieve the necessary deceleration [20].

The cases under investigation in previous work [20,22], had small ΔVs so the tether mass was assumed to be very small. The consequences of extending the sliding pendulum theory to include massive tethers are the same as in the vertical impact theory: the equation for the tether mass becomes transcendental and the tensions (and hence the tether mass approximations) at the probe and orbiter are not equal. Furthermore, normal forces in the tether must now be taken into account.

The generalized coordinates for the sliding pendulum system (shown in Fig. 7) are the orientation angle, α, and the location of the sliding attachment point (orbiter). The equations of motion [20] are:

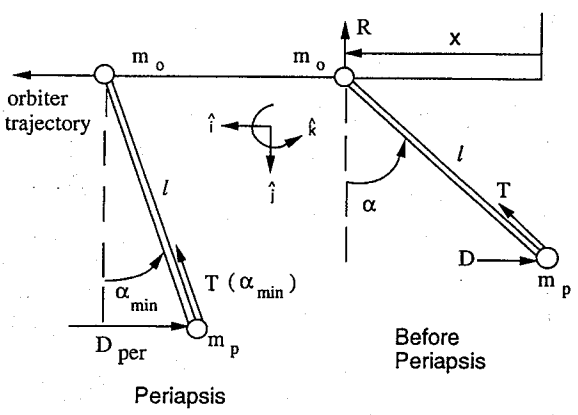

Fig. 7. Sliding pendulum model.

$$\ddot{\alpha} = \frac{-ml_o l_p\dot{\alpha}^2\cos\alpha\sin\alpha + l_p D\cos\alpha}{ml_o^2\sin^2\alpha + I}$$

$$\ddot{x} = D\left(\frac{l_o l_p\cos^2\alpha}{ml_o^2\sin^2\alpha + I} - \frac{1}{m}\right) - l_o\dot{\alpha}^2\sin\alpha\left(1 + \frac{ml_o l_p\cos^2\alpha}{ml_o^2\sin^2\alpha + I}\right) \tag{16}$$

where the drag force, D, applied to the probe end of the pendulum is

$$D = D_{\text{per}}\exp[l(\cos\alpha - \cos\alpha_{\min})/H] \tag{17}$$

and where H is the scale height and l is the length of the pendulum. The magnitude of the drag force at periapsis, D_{per}, is approximated by an impulse analysis for a particle [20] as

$$D_{\text{per}} = m\Delta V\sqrt{\frac{r_{\text{per}}e}{2\pi H r_{\text{per}}}}\frac{V_{lc}}{} \tag{18}$$

where r_{per} is the radius (of the center of mass) at periapsis, e is the eccentricity of approach and V_{lc} is the local circular velocity at r_{per}.

The acceleration of the probe, $\ddot{\mathbf{R}}_{\mathbf{p}}$, and the orbiter, $\ddot{\mathbf{R}}_{\mathbf{o}}$, are given by [20]

$$\ddot{\mathbf{R}}_{\mathbf{p}} = (\ddot{x} - l\ddot{\alpha}c_\alpha + l\dot{\alpha}^2 s_\alpha)\hat{\mathbf{i}} - (l\ddot{\alpha}s_\alpha + l\dot{\alpha}^2 c_\alpha)\hat{\mathbf{j}};$$

$$\ddot{\mathbf{R}}_{\mathbf{o}} = \ddot{x}\hat{\mathbf{i}} \tag{19}$$

where s_α and c_α represent sin α and cos α, respectively. Then applying Newton's second law to each of these particles we obtain

Probe end:

$$T_p s_\alpha + N_p c_\alpha - D = m_p(\ddot{x} - l\ddot{\alpha}c_\alpha + l\dot{\alpha}^2 s_\alpha)$$

$$T_p c_\alpha + N_p s_\alpha = -m_p(l\ddot{\alpha}s_\alpha + l\dot{\alpha}^2 c_\alpha). \tag{20}$$

Orbiter end:

$$-T_o s_\alpha + N_o c_\alpha = m_o\ddot{x}$$

$$T_o c_\alpha + N_o s_\alpha - R = 0 \tag{21}$$

where T_p and T_o are the tensions at the probe and orbiter and N_p and N_o are the normal forces (in the $\hat{\mathbf{i}}$ direction at $\alpha = 0°$) at the probe and orbiter, respectively. The force, R, at the orbiter is caused by the reaction that is needed to constrain the motion of the pendulum sliding attachment point to a horizontal line. This constraint force is solved for by applying Newton's Law and Euler's Law to the system to get [20]

$$R = ml_o(\ddot{\alpha}s_\alpha + \dot{\alpha}^2 c_\alpha). \tag{22}$$

Solving Eqs. (20) and (21) for the tensions and normal forces (at both the probe and orbiter ends of the tether) and substituting for R yields

Probe end:

$$T_p(\alpha, \dot{\alpha}) = Ds_\alpha + m_p s_\alpha \ddot{x} + m_p l\dot{\alpha}^2 \tag{23}$$

$$N_p(\alpha, \dot{\alpha}) = Dc_\alpha + m_p c_\alpha \ddot{x} - m_p l\ddot{\alpha}. \tag{24}$$

Orbiter end:

$$T_o(\alpha, \dot{\alpha}) = -m_o s_\alpha \ddot{x} + ml_o c_\alpha(\ddot{\alpha}s_\alpha + \dot{\alpha}^2 c_\alpha) \tag{25}$$

$$N_o(\alpha, \dot{\alpha}) = m_o c_\alpha \ddot{x} + ml_o s_\alpha(\ddot{\alpha}s_\alpha + \dot{\alpha}^2 c_\alpha). \tag{26}$$

Note that these forces can be written explicitly in terms of α and $\dot{\alpha}$ by substitution of Eqs. (16) and (17). For the case where $m_t = 0$, Eqs. (24) and (26) are equal to zero, confirming the analysis for small tethers which excluded normal forces. For the massive tethers, however, these forces are nonzero and must be included in the modeling to achieve satisfactory results.

Following [20,22], we adopt the hypothesis (based on experience with numerically obtained solutions) that the minimum-mass maneuver maintains a nearly constant tension during the atmospheric fly-through. By evaluating eqn (23) (or eqn (25)) at two points in the atmosphere and equating the resulting expressions, we obtain a transcendental formula for the minimum orientation angle, $\alpha_{\min}$, which approximates the value for the optimum inclined maneuver.

We have closed-form expressions for $\dot{\alpha}$ when $\alpha = \alpha_{\min}$ and when the spin rate has not been altered significantly from the value it has outside the atmosphere (where we assume $\alpha = 90°$). At $\alpha = \alpha_{\min}$ we have

$$\dot{\alpha} = 0. \tag{27}$$

At $\alpha = 90°$ we have

$$\dot{\alpha} = \dot{\alpha}_{\text{imp}} = m\Delta V l_p \cos\alpha_{\min}/(2I) \tag{28}$$

where $\dot{\alpha}_{\text{imp}}$ is obtained using impulse theory as in eqn (5). We can now evaluate the tensions (at the probe) for these two points of the fly-through trajectory by substituting Eqs. (16), (17), (27) and (28) into eqn (23) (and, likewise, into eqn (25) for the orbiter):

Probe end:

$$T_p(\alpha_{\min}, 0) = \frac{\Delta V V_{lc}\sqrt{e}}{\sqrt{2\pi r_{\text{per}}\bar{H}}} \times \left[ms_m + m_p s_m\left(\frac{ml_o l_p}{ml_o^2 s_m^2 + I}c_m^2 - 1\right)\right] \tag{29}$$

$$T_p(90°, \dot{\alpha}_{\text{imp}}) = \frac{\Delta V V_{lc}\sqrt{e}}{\sqrt{2\pi r_{\text{per}}\bar{H}}}(m - m_p)\, e^{(-l c_m)/H} + \frac{m_p m^2 l_p^2}{4\bar{I}^2}(l - l_o)c_m^2 \Delta V^2. \tag{30}$$

Orbiter end:

$$T_o(\alpha_{\min}, 0) = \frac{\Delta V V_{lc}\sqrt{e}}{\sqrt{2\pi r_{\text{per}}\bar{H}}} \left[m_o s_m + (m - m_o)\left(\frac{ml_o l_p s_m c_m^2}{ml_o^2 s_m^2 + I}\right)\right] \tag{31}$$

$$T_o(90°, \dot{\alpha}_{\text{imp}}) = \frac{m_o \Delta V V_{lc}\sqrt{e}}{\sqrt{2\pi r_{\text{per}}\bar{H}}}\, e^{(-l c_m)/H} + \frac{m^2 l_o l_p^2}{4I^2}c_m^2 \Delta V^2 \tag{32}$$

where s_m and c_m represent $\cos\alpha_{\min}$ and $\sin\alpha_{\min}$, respectively.

We equate the two tensions at the probe in Eqs. (29) and (30) (and Eqs. (31) and (32) for the orbiter) and use the nondimensional parameters from (8) and (9) to obtain an equation that governs $\alpha_{\min}$.

Probe end:

$$f_p(\bar{m}_{tp}, \alpha_{\min}, m_r, \bar{h}_c, u) = \bar{m}s_m + m_r s_m \times \left(\frac{\bar{m}\bar{l}_o\bar{l}_p}{\bar{m}\bar{l}_o^2 s_m^2 + \bar{I}}c_m^2 - 1\right) - (\bar{m} - m_r)\, e^{-\bar{h}_c} + \frac{m_r \bar{m}^2 \bar{l}_p^2}{4\bar{h}_c\bar{I}^2} \times (1 - \bar{l}_o)c_m^3 u = 0. \tag{33}$$

Orbiter end:

$$f_o(\bar{m}_{to}, \alpha_{\min}, m_r, \bar{h}_c, u) = s_m + (\bar{m} - 1)\frac{\bar{m}\bar{l}_o\bar{l}_p s_m c_m^2}{\bar{m}\bar{l}_o^2 s_m^2 + \bar{I}} - e^{-\bar{h}_c} - \frac{\bar{m}^2\bar{l}_o\bar{l}_p^2}{4\bar{h}_c\bar{I}^2}c_m^3 u = 0 \tag{34}$$

where we have defined nondimensional speed and clearance variables, respectively, to be

$$u \equiv (\Delta V/V_{lc})\sqrt{2\pi r_{\text{per}}/(He)}$$
$$\bar{h}_c \equiv h_c/H \tag{35}$$

where h_c is the clearance required between the minimum altitude of the orbiter and the minimum altitude of the probe. In eliminating the tether length, l, from Eqs. (33) and (34) we have assumed, as in [20,22], that the tether length is just long enough

for the required clearance to be achieved. This dependence on clearance can be expressed as

$$l = h_c / \cos \alpha_{\min}. \tag{36}$$

Neglecting the tether mass (i.e. setting $\bar{m}_t = 0$) in Eqs. (33) and (34), yields an identical result for both probe and orbiter, namely, the $\alpha_{\min}$ expression found using the small tether theory [22]:

$$\frac{1}{s_m}\left[1 - \left(\frac{c_m^2}{1 + m_r s_m^2}\right)\right] - \exp(-\bar{h}_c) - \frac{1}{4}\left(\frac{1 + m_r}{m_r}\right)\frac{u}{\bar{h}_c} c_m^3 = 0. \tag{37}$$

Since $\bar{m}_t$ does not appear in eqn (37), we can directly solve for the optimal $\alpha_{\min}$ (e.g. using a root finder), given m_r, $\bar{h}_c$ and u. A scaled tether mass can then be calculated that is dependent on the three parameters, m_r, $\bar{h}_c$ and u. Consequently, the optimal mass problem for small tethers is a function of only three parameters [22]. For the large tether theory, however, Eqs. (33) and (34) are coupled with the expression for the tether mass. This expression is found using the maximum tension at the probe (and obiter) as follows:

$$\bar{m}_{tp} = T_p(\alpha_{\min}, 0) l \rho / \sigma = \frac{\bar{h}_c \Delta V^2 \rho}{u c_m \sigma} \times \left[\bar{m} s_m + m_r s_m \left(\frac{\bar{m}\bar{l}_o \bar{l}_p}{\bar{m}\bar{l}_o^2 s_m^2 + \bar{I}}\, c_m^2 - 1\right)\right] \tag{38}$$

$$\bar{m}_{to} = T_o(\alpha_{\min}, 0) l \rho / \sigma = \frac{\bar{h}_c \Delta V^2 \rho}{u c_m \sigma} \times \left[s_m + (\bar{m} - 1)\frac{\bar{m}\bar{l}_o \bar{l}_p s_m c_m^2}{\bar{m}\bar{l}_o^2 s_m^2 + \bar{I}}\right]. \tag{39}$$

Equation (38) is solved simultaneously with eqn (33) to get a solution for the optimum $\alpha_{\min}$ and $\bar{m}_{tp}$. (Similarly, eqn (39) is simultaneously solved with eqn (34) to find $\bar{m}_{to}$.) Not only does this add to the difficulty of solving the equations, but it introduces another independent parameter into the problem, namely ΔV. Thus, the optimal mass problem for massive tethers is a *four-parameter problem* (m_r, $\bar{h}_c$, u and ΔV) for a given tether material. For convenience, we remove ΔV from the parameter u to create a new parameter, $\tilde{u}$, that is a function of planetary parameters and the approach trajectory:

$$\tilde{u} \equiv \sqrt{2\pi r_{\text{per}}/(He)}/V_{lc}. \tag{40}$$

Then, rewriting Eqs. (33) and (38), the solution for $\alpha_{\min}$ and $\bar{m}_{tp}$ is found by simultaneously solving

$$\bar{m} s_m + m_r s_m \left(\frac{\bar{m}\bar{l}_o \bar{l}_p}{\bar{m}\bar{l}_o^2 s_m^2 + \bar{I}}\, c_m^2 - 1\right) - (\bar{m} - m_r)\, \mathrm{e}^{-\bar{h}_c} + \frac{m_r \bar{m}^2 \bar{l}_p^2}{4\bar{h}_c \bar{I}^2}(1 - \bar{l}_o) c_m^3 \tilde{u} \Delta V = 0$$

$$\bar{m}_{tp} - \frac{\bar{h}_c \Delta V \rho}{\tilde{u} c_m \sigma}\left[\bar{m} s_m + m_r s_m \left(\frac{\bar{m}\bar{l}_o \bar{l}_p}{\bar{m}\bar{l}_o^2 s_m^2 + \bar{I}}\, c_m^2 - 1\right)\right] = 0. \tag{41}$$

Similarly, from Eqs. (34) and (39), the solution for $\alpha_{\min}$ and $\bar{m}_{to}$ is found by solving

$$s_m + (\bar{m} - 1)\frac{\bar{m}\bar{l}_o \bar{l}_p s_m c_m^2}{\bar{m}\bar{l}_o^2 s_m^2 + \bar{I}} - \mathrm{e}^{-\bar{h}_c} - \frac{\bar{m}^2 \bar{l}_o \bar{l}_p^2}{4\bar{h}_c \bar{I}^2}\, c_m^3 \tilde{u} \Delta V = 0$$

$$\bar{m}_{to} - \frac{\bar{h}_c \Delta V \rho}{\tilde{u} c_m \sigma}\left[s_m + (\bar{m} - 1)\frac{\bar{m}\bar{l}_o \bar{l}_p s_m c_m^2}{\bar{m}\bar{l}_o^2 s_m^2 + \bar{I}}\right] = 0. \tag{42}$$

Since the tether has uniform diameter and must be made to withstand the maximum tension between the probe and orbiter, the final estimate of the optimum tether mass is the larger of the two estimates given by the expressions above. That is

$$\bar{m}_t = \max\{\bar{m}_{tp}, \bar{m}_{to}\}. \tag{43}$$

Values for $\tilde{u}$ are given in Tables 1 and 2 for the major atmosphere-bearing bodies in the solar system. The approach eccentricity, e, is calculated for the hyperbolic trajectory with respect to the target planet, resulting from a Hohmann transfer from Earth (or from Mars when Earth is the target planet). The scale heights and planetary gravitational parameters are given in [16]. The periapsis radii can be approximated by the radii of the planets. Note that the $\tilde{u}$s fall into two distinct categories made up by the *gas giants* and the *terrestrial* planets. (While the astute reader will observe that Titan is not even a planet, much less a gas giant, its thick atmosphere places it within this category for the purposes of aerobraking tether design.) We now investigate a candidate from each of these categories, since,

Table 1. Gas giants

Planet	$\tilde{u}$
Jupiter	3.453
Neptune	3.751
Uranus	4.214
Saturn	4.417
Titan	4.754

Table 2. Terrestrials

Planet	$\tilde{u}$
Venus	10.41
Earth	10.75
Mars	11.91

theoretically, there are really only two cases (either $\tilde{u} \approx 4$ or $\tilde{u} \approx 11$).

5. RESULTS

The optimal tether mass predicted by the vertical impact theory in eqn (14) and the optimal tether mass predicted by the sliding pendulum theory in eqn (43) are plotted as solid lines in Fig. 8 for varying ΔVs at Jupiter (where $\tilde{u} = 3.453$). We assume that the probe and orbiter have equal mass (so that $m_r = 1$) and that a clearance of 1.8 scale heights is required between the orbiter and the probe (i.e. $\bar{h}_c = 1.8$). We assume the tether material, Hercules AS4, has the following characteristics [16]:

$$\rho = 1800 \text{ kg/m}^3, \quad \sigma = 3.6 \text{ GN/m}^2. \tag{44}$$

The minimum-mass tether is given by the *lower value* predicted by the vertical impact and sliding pendulum theories. For instance in Fig. 8, at a ΔV of 1.5 km/s, the optimal-mass tether is approximated by the sliding pendulum theory to be about 0.7 times the mass of the orbiter. The lower curve also indicates what type of maneuver is required for the lowest tether mass. Thus, for ΔVs between 0 and 0.92 km/s the optimal-mass maneuver is expected to be a vertical dumb-bell maneuver since the vertical impact theory yields the lowest tether mass. For ΔVs greater than 0.92 km/s, an inclined maneuver is optimal, as predicted by the sliding pendulum theory.

To test these predictions we numerically optimize the maneuver using the tether equations of motion with distributed aerodynamic and gravitational forces [14]. (Note: these equations of motion are far too lengthy to include in this paper.) The optimization is accomplished by mapping the tether mass as discussed in the introduction and in [22]. Five different maneuvers were optimized at Jupiter and are indicated by asterisks in Fig. 8. The ΔVs for these maneuvers are 0.2686, 1.017, 1.393, 1.775 and 2.002 km/s and the corresponding final eccentricities, e_f, are 0.9999, 0.9500, 0.9250, 0.9000 and 0.8850, respectively. The approach eccentricity is 1.018 in all cases (associated with the $\tilde{u}$ given above). The numerical values for the minimum tether mass match very closely with the theoretical values. The type of maneuver is also well predicted by the theories: the numerical solution for the ΔV of 0.2686 km/s is a vertical dumb-bell maneuver and all the others are inclined maneuvers.

The usefulness of extending the theories to include massive tethers is clearly shown in Fig. 8. The tether mass values using the small tether theory are plotted as short dashed lines for both the vertical impact (eqn (15)) and the sliding pendulum [22] theories. For ΔVs where the tether mass is more than about a third of the orbiter mass (i.e. for $\Delta V > 1.1$ km/s), the massive theory diverges signifi-

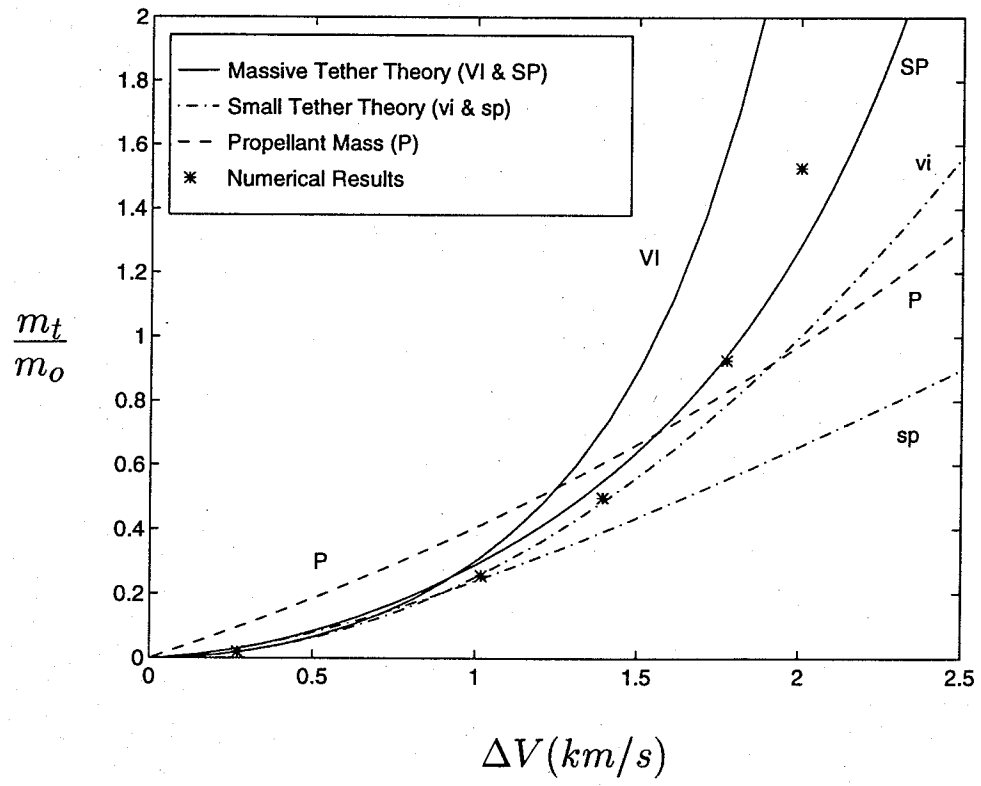

Fig. 8. Theoretical and numerical tether masses at Jupiter.

cantly from the small mass theory and provides much better results.

The merit of the aerobraking tether can be partially assessed by comparing the optimal-mass predictions with the propellant required to achieve an identical ΔV on the orbiter (without the use of any aerobraking). The propellant mass, m_{prop}, is easily determined using the rocket equation:

$$m_{\text{prop}} = m_o\left[\exp\left(\frac{\Delta V}{I_{\text{sp}}g}\right) - 1\right] \tag{45}$$

where the acceleration due to Earth's gravity, g, is assumed to be standard freefall (9.80665 m/s^2) and the specific impulse, I_{sp}, is assumed to be 300 s. The propellant mass in Fig. 8 is greater than the tether mass for ΔVs below about 1.55 km/s (where $e_f = 0.915$), showing that aerobraking tethers have a mass savings over a wide range of maneuvers. Since the analytic theory is accurate for this entire range of ΔVs, the massive tether theory is an excellent tool for preliminary design at Jupiter.

When comparing the numerical results to the sliding pendulum theory, we find that the $\Delta V = 0.2686$, 1.017 and 1.393 km/s cases are slightly below the curve, the $\Delta V = 1.775$ km/s case is almost exactly on the curve, and the $\Delta V = 2.002$ km/s case is significantly higher than the sliding pendulum theory. The excellent correlation between the analytic theory and numerical solution at $\Delta V = 1.775$ km/s seems to be related to the flatness of the orbiter's trajectory when the numerically optimized maneuver is simulated. Figure 9 shows the time histories of the radial distances from the center of Jupiter to both the orbiter and probe. During the atmospheric fly-through (about 210 to 295 s), the altitude of the orbiter only changes by about 4.5 km while the probe swings down more than 40 km to achieve the necessary aerodynamic braking. This behavior constitutes the ideal sliding pendulum motion: the orbiter maintains a nearly constant altitude, while the probe swings down, collides with the atmosphere (at $\alpha_{\text{min}} = 30.1°$) and bounces back out of the atmosphere. Hence, it is reasonable to expect that the theory is most accurate for this case.

Figure 10 provides further evidence for the conjecture that flatness in the orbiter trajectory is an indicator of when the sliding pendulum theory is most accurate. Here, the orbiter trajectories are plotted for all five of the numerically optimized maneuvers discussed above. The duration of the atmospheric fly-through and the shape of the probe's trajectory are very close in all these cases. The $\Delta V = 2.002$ km/s case, where the sliding pendulum prediction is lower than the actual value, has an irregularly shaped orbiter trajectory. For this example, the motion seems fundamentally different from the cases with lower ΔV in which the orbiter height monotonically decreases as it approaches periapsis and then monotonically increases as it leaves periapsis. As we will see in the Mars results,

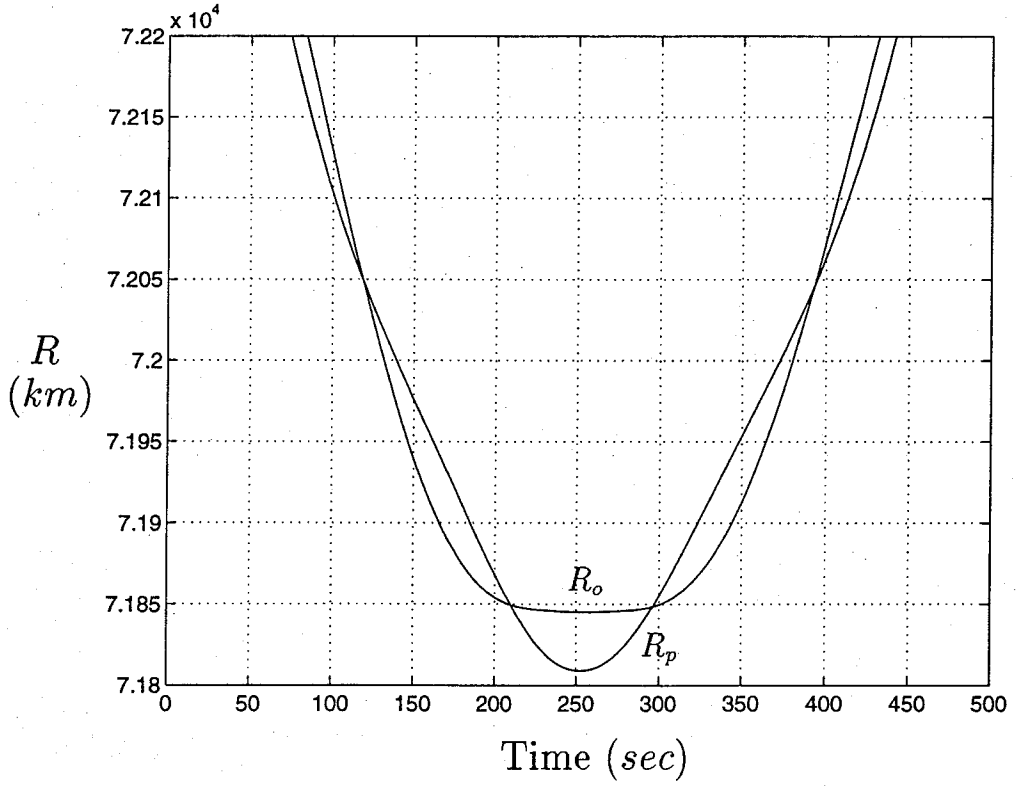

Fig. 9. Orbiter and probe radii for $\Delta V = 1.775$ km/s.

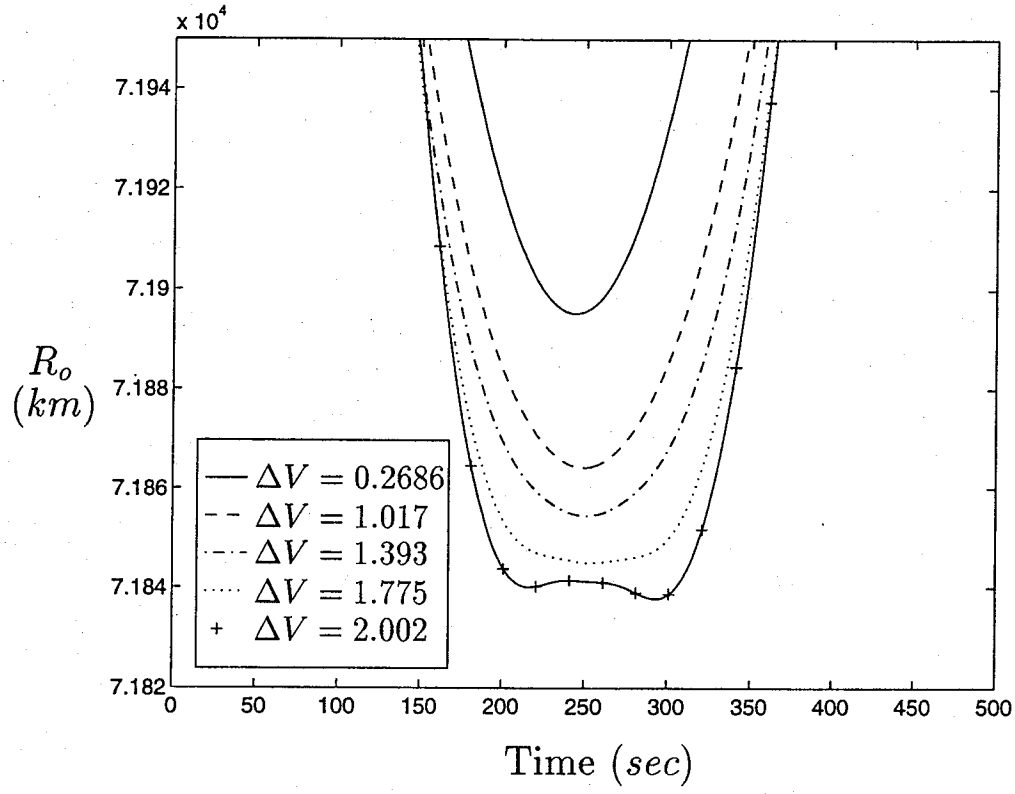

Fig. 10. Orbiter radii for different ΔVs at Jupiter.

an irregularly shaped orbiter trajectory, like that of the $\Delta V = 2.002$ km/s case, seems to be an indicator of when the sliding pendulum theory breaks down.

In Fig. 11, a history of the tension at the probe end of the tether is plotted for each of the numerically optimized examples. (The shape of the ten-

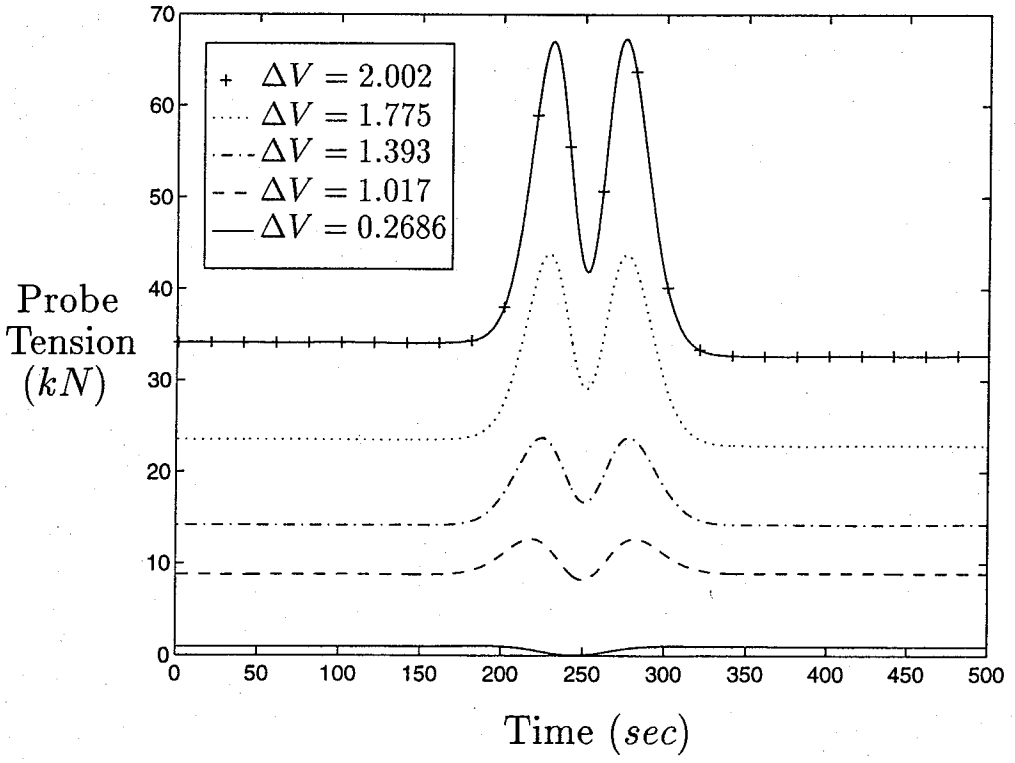

Fig. 11. Tension histories for different ΔVs at Jupiter.

sions are similar to the orbiter, but the magnitudes are different.) The plots exhibit the same classic behavior shown in Figs 4 and 5. For instance, the $\Delta V = 0.2686$ km/s case has a vertical dumb-bell tension history characterized by vanishing tension at periapsis (when $t \approx 250$ s). The tension histories of the other cases have the shape of the classic inclined maneuver, namely, nearly equal tensions before and after atmospheric fly-through (due to spin rate) with two humps during the aerobraking maneuver caused by a combination of spin rate and aerodynamic drag. The tension profiles demonstrate that increasing ΔV causes the optimal maneuver to transition from a vertical dumb-bell to an inclined maneuver. Note that the spin tensions start to become slightly asymmetric for the case where $\Delta V = 2.002$ km/s (where spin rate after atmospheric impact is 96% of the spin rate before impact). This asymmetry seems to accompany the irregularly shaped orbiter trajectory discussed above.

The theoretical tether mass from the sliding pendulum model for varying ΔV at Mars ($\tilde{u}=11.91$) is plotted in Fig. 12. For clarity, the results for the vertical impact model are not shown since they only yield lower tether masses for ΔVs below 0.25 km/s (or $e_f > 1.35$) where the two curves are indistinguishable on the given scale. Thus, the optimal maneuver is predicted to be inclined for any aerocapture maneuver ($e_f < 1.0$).

Again, we use numerically optimized cases to test the merit of the analytic theory. The asterisks in Fig. 12 are at ΔVs of 0.6636, 0.9180, 1.187, 1.328 and 1.548 km/s which correspond to final eccentricities of 0.9999, 0.8000, 0.6000, 0.5000 and 0.3500. The approach eccentricity is 1.571. All of these maneuvers are inclined (but not necessarily in the classic sense, as is shown below) so the maneuver type is correctly predicted by the theory. Unfortunately, the theoretical values for the optimal tether mass become progressively worse as ΔV is increased. In fact, the massive tether theory has little use at Mars (for this $\tilde{u}$). At low ΔVs, where predictions are accurate, the large tether theory is nearly the same as the small tether theory; at high ΔVs the massive tether theory yields a small improvement in accuracy, but it is still a poor predictor.

The sliding pendulum curve (for massive tethers) intersects the propellant curve of Fig. 12 at 4.8 km/s, implying that the tether has a mass savings for ΔVs below this value. (Note that this intersection is not actually shown on the plot.) The numerical results, however, show that this crossing actually occurs at a much smaller velocity change. Using a polynomial curve fit, the break-even point between the propellant and tether mass is at about 1.46 km/s (where $e_f = 0.409$). Fortunately, this range of ΔVs encompasses a wide range of final eccentrici-

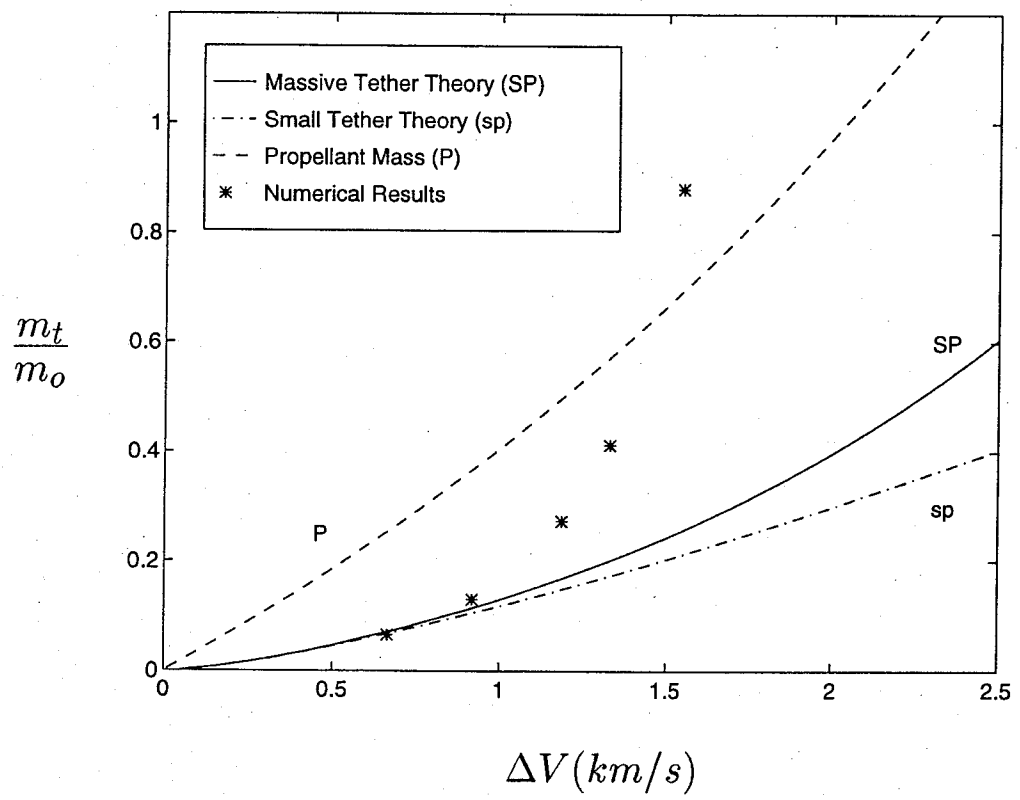

Fig. 12. Theoretical and numerical tether masses at Mars.

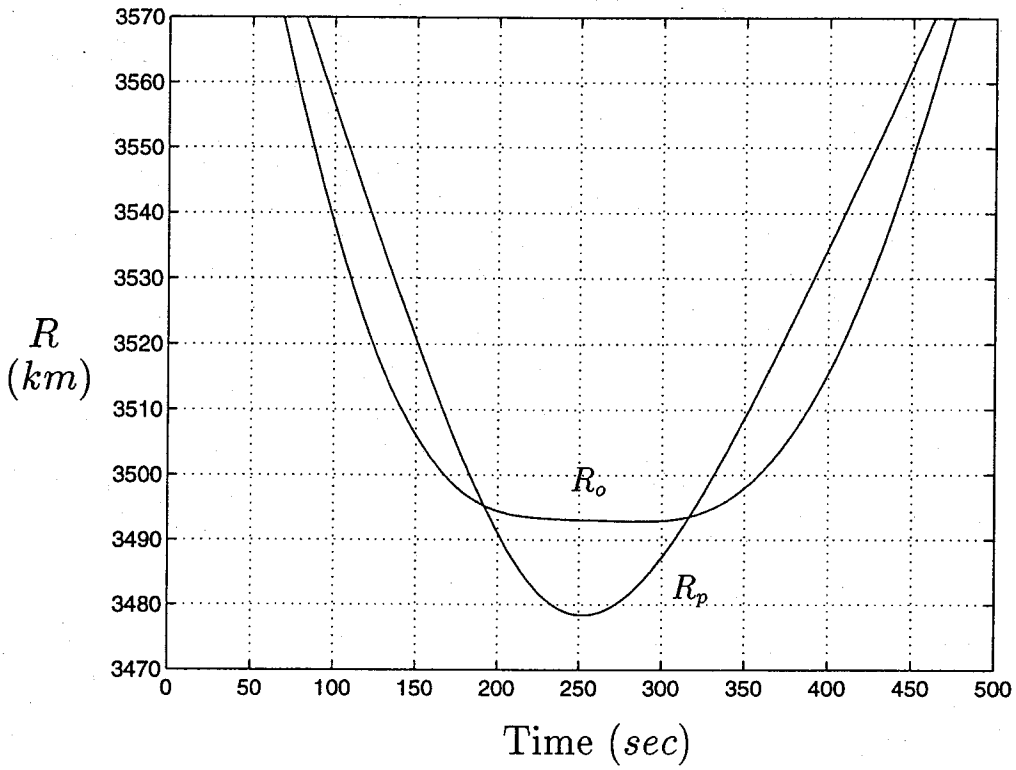

Fig. 13. Orbiter and probe radii for $\Delta V = 0.6636$ km/s.

ties, making the aerobraking tether an attractive prospect for terrestrial planets as well.

The divergence between theoretical and numerical values at Mars is puzzling, particularly in light of the success attained at Jupiter. One possible explanation could be the low values for the final eccentricities. The numerical examples at Jupiter all had final eccentricities greater than 0.8850, but at Mars four out of the five cases were *below* this final eccentricity and involve somewhat different dynamics

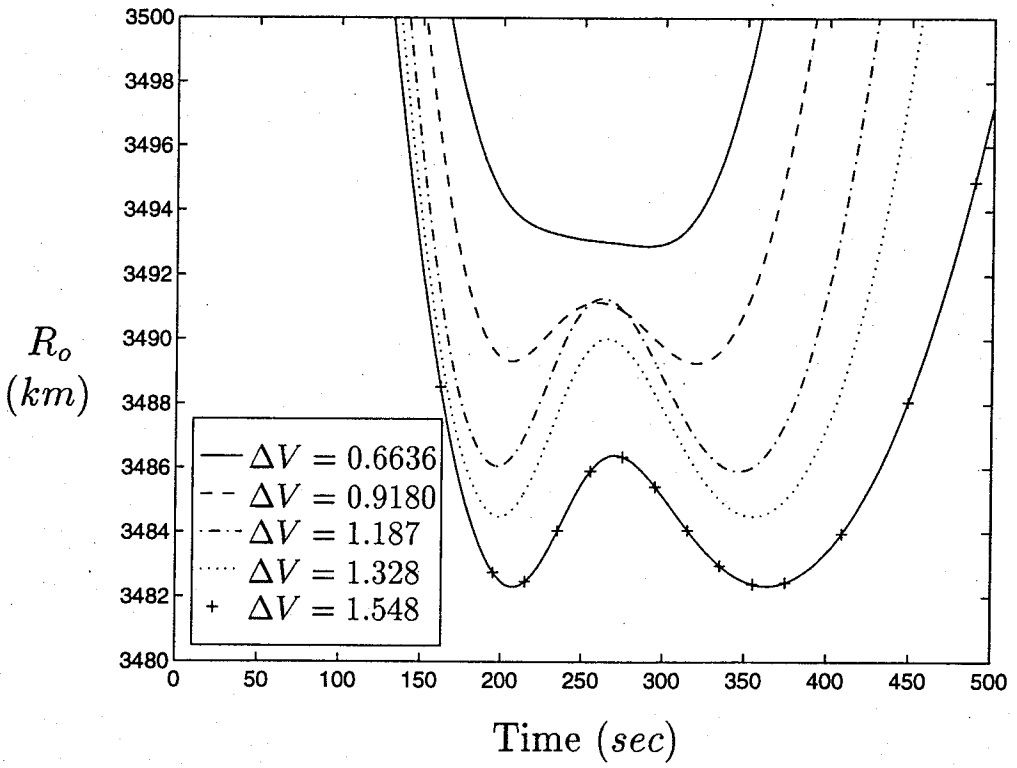

Fig. 14. Orbiter radii for different ΔVs at Mars.

(such as a slightly longer fly-through time and a much flatter exit trajectory).

To study the effect of final eccentricity, the approach eccentricity was increased (which decreased $\tilde{u}$) for each case such that the previous five ΔVs resulted in a fixed final eccentricity of 0.9999. We found that the change in the $\tilde{u}$ for each case raised the theoretical sliding pendulum prediction while the tether mass for the numerical value decreased. Thus, the accuracy of the theory can be improved a bit when we constrain the final orbit to have $e_f = 0.9999$, but the discrepancy between the numerical solutions and the analytic theory is still nearly as large as in Fig. 12. We conclude that the final eccentricity is only a second-order effect and that the divergence is an unavoidable result at large $\tilde{u}$ for large ΔVs.

As illustrated by the Jupiter example, the orbiter trajectory can serve as an indicator of when the analytic theory will be accurate. The best correlation between predicted and actual tether mass values occurs at a ΔV of 0.6636 km/s (where $e_f = 0.9999$). The orbiter and probe trajectories are plotted for this example in Fig. 13. The radial distance to the orbiter is relatively constant during the aerobraking portion of the maneuver which is ideal behavior as modeled by the sliding pendulum.

The other cases at Mars are shown in Fig. 14 and have irregularly shaped orbiter profiles with two local minima and nonconstant orbiter altitudes, just as the $\Delta V = 2.002$ km/s case did at Jupiter. All the cases at Mars with this oscillatory behavior have sliding pendulum tether mass predictions that are much lower than the numerical values. (The exception at $\Delta V = 0.9180$ km/s is accurately predicted despite oscillatory behavior in the orbiter trajectory, but the altitude is still fairly constant, varying by less than 2 km during fly-through). Note that this behavior is not modeled by the sliding pendulum equations of motion, so inaccurate results seem to be inevitable. Furthermore, the assumption employed in eqn (36) is now invalid since the clearance altitude can no longer be approximated at periapsis due to the large loss in the orbiter altitude before and after periapsis passage.

The tension histories in Fig. 15 all have characteristics of the inclined maneuver: low spin tension outside of the atmosphere and large tension during fly-through due to a combination of spin rate and aerodynamic drag. However, only the $\Delta V = 0.6636$ km/s case has a classic profile characterized by nearly equal exoatmospheric tensions and symmetric maxima during the aerobraking portion of maneuver. As mentioned above, the asymmetries in tension seem to be correlated with the oscillatory orbiter trajectory near closest approach and, hence, with inaccurate results from the sliding pendulum model.

6. CONCLUSIONS

The optimal mass theory developed here for the massive tether provides very accurate results for aerocapture at the gas giants. In the case of the terrestrial planets, however, the theory diverges and

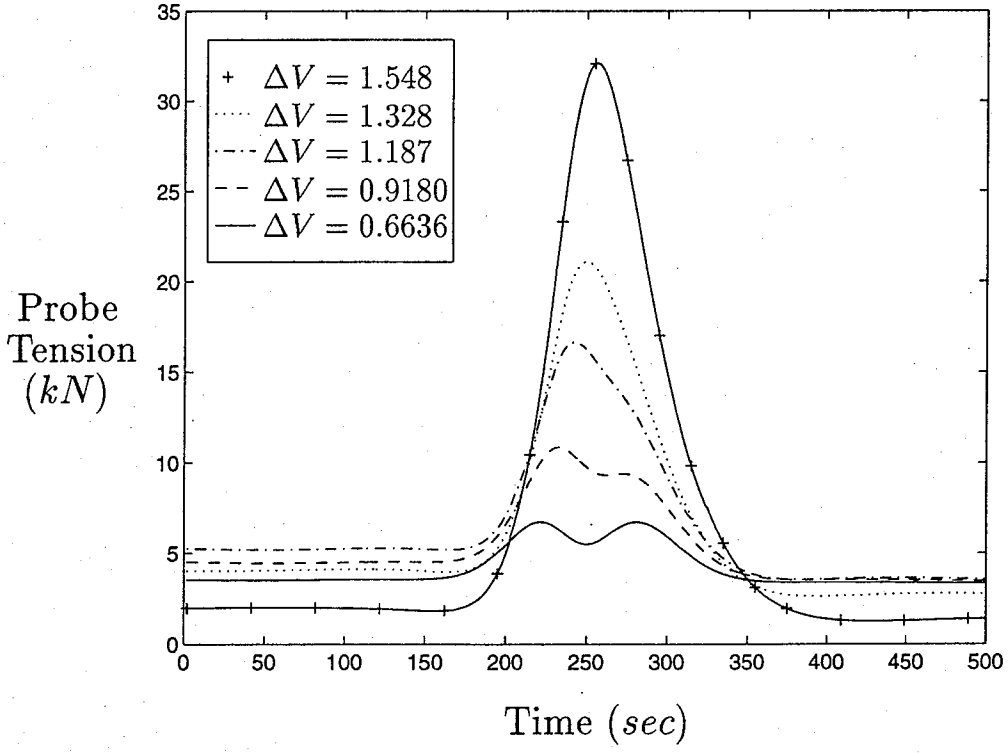

Fig. 15. Tension histories for different ΔVs at Mars.

we must resort to numerical techniques for large ΔV. The theory for massive tethers is characterized by only four parameters which greatly simplifies the analysis. (In the case of small tethers, the theory reduces even further, requiring only three parameters for a complete description.) These concepts, coupled with the work presented previously, provide some guiding principles in the design of aerobraking tethers.

REFERENCES

1. Carroll, J.A., *Acta Astronautica*, 1986, **13,** 165–174.
2. Sirlin, S. W., Laskin, R. A., Otake, H. and Longuski, J. M., in *Proposal to JPL director's discretionary fund FY'84: tethers for aerocapture and trajectory maneuvers.* Jet Propulsion Laboratory, Pasadena, CA, 1984.
3. Purvis, C. and Penzo, P., in *Tethers in space handbook.* Office of Space Flight Advanced Programs (NASA), Washington, DC, 1986, pp. 3.63–3.64.
4. Lorenzini, E., Grossi, M.D. and Cosmo, M., *Acta Astronautica*, 1990, **21,** 1–12.
5. Bergamaschi, S. and Bonon, F., in *AAS/AIAA Astrodynamics Conference.* AAS-91-543, Durango, CO, 1991.
6. Keshmiri, M. and Misra, A. K., in *AAS/AIAA Spaceflight Mechanics Meeting.* AAS-93-184, Pasadena, CA, 1993.
7. Gullahorn, G. 1989. *Third International Conference on Tethers in Space Toward Flight.* Paper 89-1566-CP, San Francisco, CA.
8. Krischke, M., Lorenzini, E. and Sabath, D. 1992. *43rd IAF Congress.* IAF-92-0822, Washington, DC.
9. Pasca, M. and Lorenzini, E.C., *AAS/AIAA Spaceflight Mechanics Meeting*, 1991, AAS–91-178, Houston, TX.
10. Bae, G., Sim, E. and Barlow, J.B., *AAS/AIAA Spaceflight Mechanics Meeting*, 1993, AAS–93-185, Pasadena, CA.
11. Warnock, T.W. and Cochran, J.E., *43rd IAF Congress*, 1992, , IAF–92-0002, Washington, DC.
12. Penzo P.A., Ammann P.W. (editors) 1989. *Tethers in space handbook.* 2nd edn. Office of Space Flight Advanced Programs, NASA, Washington, DC.
13. Beletsky, V. V. and Levin, E. M. 1993. *Dynamics of space tether systems.* American Astronautical Society, San Diego, CA.
14. Puig-Suari, J. and Longuski, J.M., *Acta Astronautica*, 1991, **25,** 679–686.
15. Longuski, J. M. and Puig-Suari, J., in *42nd IAF Congress.* IAF-91-339, Montreal, Canada, 1991.
16. Puig-Suari, J., Longuski, J.M. and Mechalas, J., *Acta Astronautica*, 1995, **35,** 205–214.
17. Puig-Suari, J. 1993. Aerobraking tethers for the exploration of the solar system. Ph.D. thesis, School of Aeronautics and Astronautics, Purdue University, West Lafayette, IN.
18. Puig-Suari, J., Longuski, J.M. and Tragesser, S.G., *Journal of Guidance, Control, and Dynamics*, 1995, **18,** 1305–1312.
19. Puig-Suari, J., *4th International Conference on Tethers in Space,* Washington, DC, 1995, 1441–1450.
20. Longuski, J.M., Puig-Suari, J., Tsiotras, P. and Tragesser, S., *Acta Astronatica*, 1995, **35,** 489–500.
21. Tragesser, S. G., Longuski, J. M., Puig-Suari, J. and Mechalas, J. P. *AIAA/AAS Astrodynamics Conference.* AIAA-94-3747, Scottsdale, AZ, 1994.
22. Tragesser, S.G., Longuski, J.M. and Puig-Suari, J., *4th International Conference on Tethers in Space,* Washington, DC, 1995, 1217–1231.
23. Tragesser, S. G., Longuski, J. M. and Puig-Suari, J., in *AAS/AIAA Astrodynamics Conference.* AAS-95-353, Halifax, Nova Scotia, Canada, 1995.
24. Puig-Suari, J., Longuski, J.M. and Tragesser, S.G., *Acta Astronautica*, 1995, **36,** 291–295.